Thermocouples from Electrodeposited Submicrometer Wires Prepared by Electrochemical Step Edge Decoration

M. E. Bourg,[†] W. E. van der Veer,[†] A. G. Güell,[‡] and R. M. Penner*,[†]

Department of Chemistry and Institute for Surface and Interface Science, University of California, Irvine, California 92697-2025, and Department of Physical Chemistry, The University of Barcelona, Martí i Franquès 1, E-08028 Barcelona, Spain

Received February 27, 2008. Revised Manuscript Received May 19, 2008

We describe the preparation of three types of silver/nickel thermocouples (TCs) based upon electrodeposited wires with diameters at, or just below, 1.0 μm: *Type 1*—wire/thin film TCs consisting of an electrodeposited submicrometer diameter wire and an evaporated metal thin film; *Type 2*—wire-wire TCs consisting of end-butted and electrochemically welded silver and nickel submicrometer wires; *Type 3*—wire-wire TCs for which the silver wires were electrochemically etched prior to the electrodeposition of the nickel wires. The metal wires in all devices were prepared using the electrochemical step edge decoration method. The properties of these TCs for measuring temperature in the range from ambient to 110 °C were evaluated. Output voltage, V_{TC}, versus temperature was linear for these devices yielding Seebeck coefficients of 19-22 μV/°C—within 95% of the expected bulk value. Temperature excursions across a 90 °C range caused no measurable hysteresis in V_{TC} for these devices. All three types of devices retained the ability to accurately measure temperature for months after exposure to ambient laboratory air. The response times for these TCs were measured using two different laser heating methods.

I. Introduction

Thermocouples (TCs), invented by Seebeck in the early 1800s,[1,2] continue to be the subject of research publications 200 years later. Not surprisingly, one frontier at which innovation and investigation continues today involves miniaturization. In the case of TCs, there are three reasons to miniaturize: (1) To probe small environments. The dimensions of the thermocouple determine the smallest region of space within which they can measure the temperature. There is increasing interest in probing temperature in the diminutive spaces enclosed by microfabricated channels,[3–7] on MEMS[8] platforms, e.g.,[9,10] within micro- and nanoparticles,[11–13] and within living cells.[14,15](2) To measure small heat fluxes. The heat capacity of a TC is directly proportional to its mass and progressive miniaturization renders a TC useful as a transducer for measuring minute heat fluxes associated with biological processes and chemical reactions—so-called "nanocalorimetry".[16–19] (3) To record rapid temperature changes. The lower heat capacity of small TCs enables faster response times for real-time monitoring of fast thermal events and fluctuations associated, for example, with turbulent combustion and detonation.[20–22]

Recent efforts aimed at reducing the response time for TCs, surveyed in Table 1, reveal the primacy of one particular fabrication approach—the creation of TCs from evaporated metal films. Such "thin film thermocouples" (TFTCs), first described by Harris and Johnson in 1933,[23] are attractive because the thermal mass of the TFTC is directly proportional to the total thickness of the metal films.

* Corresponding author. E-mail: rmpenner@uci.edu.
[†] University of California, Irvine.
[‡] The University of Barcelona.

(1) Seebeck, T. J. *Abh. K. Akad. Wiss. Berlin* **1821**, >289.
(2) Seebeck, T. J. *Abh. K. Akad. Wiss. Berlin* **1823**, 265.
(3) Chaudhari, A. M.; Woudenberg, T. M.; Albin, M.; Goodson, K. E. *J. Microelectromech. Syst.* **1998**, *7*, 345.
(4) Davis, K. L.; Liu, K. L. K.; Lanan, M.; Morris, M. D. *Anal. Chem.* **1993**, *65*, 293.
(5) Liu, K. L. K.; Davis, K. L.; Morris, M. D. *Anal. Chem.* **1994**, *66*, 3744.
(6) Ross, D.; Gaitan, M.; Locascio, L. E. *Anal. Chem.* **2001**, *73*, 4117.
(7) Ross, D.; Locascio, L. E. *Anal. Chem.* **2002**, *74*, 2556.
(8) MEMS = Micro Electro Mechanical Systems.
(9) Meyer, C. W.; Meier, D. C.; Montgomery, C. B.; Semancik, S. *Sens. Actuators, A* **2006**, *127*, 235.
(10) Semancik, S.; Cavicchi, R. E.; Wheeler, M. C.; Tiffany, J. E.; Poirier, G. E.; Walton, R. M.; Suehle, J. S.; Panchapakesan, B.; DeVoe, D. L. *Sens. Actuators, B* **2001**, *77*, 579.
(11) Lai, S. L.; Carlsson, J. R. A.; Allen, L. H. *Appl. Phys. Lett.* **1998**, *72*, 1098.
(12) Rassat, S. D.; Davis, E. J. *Appl. Spectrosc.* **1994**, *48*, 1498.
(13) Richardson, H. H.; Thomas, A. C.; Carlson, M. T.; Kordesch, M. E.; Govorov, A. O. *J. Electron. Mater.* **2007**, *36*, 1587.
(14) Gota, C.; Uchiyama, S.; Ohwada, T. *Analyst* **2007**, *132*, 121.
(15) Tseeb, V.; Suzuki, M.; Ishiwata, S. *Biophys. J.* **2005**, *88*, 343A.
(16) Fominaya, F.; Fournier, T.; Gandit, P.; Chaussy, J. *Rev. Sci. Instrum.* **1997**, *68*, 4191.
(17) Garden, J. L.; Chateau, E.; Chaussy, J. *Appl. Phys. Lett.* **2004**, *84*, 3597.
(18) Minakov, A. A.; Schick, C. *Rev. Sci. Instrum.* **2007**, *78*, 073902.
(19) Yao, H.; Ema, K.; Fukada, H.; Takahashi, K.; Hatta, I. *Rev. Sci. Instrum.* **2003**, *74*, 4164.
(20) Hung, P. C.; Irwin, G.; Kee, R.; McLoone, S. *Rev. Sci. Instrum.* **2005**, *76*, 024902.
(21) Katsuki, M.; Mizutani, Y.; Matsumoto, Y. *Combust. Flame* **1987**, *67*, 27.
(22) Alspach, D. A. *Temperature measurements through a solid-propellant combustion wave using imbedded fine wire thermocouples*; Astronaut. Lab., AFSC: Edwards AFB, CA, 1990; 29 pp.
(23) Harris, L.; Johnson, E. A. *Rev. Sci. Instrum.* **1934**, *5*, 153.

10.1021/cm800582p CCC: $40.75
Published on Web 08/08/2008

Table 1. Chronology of Rapid-Responding Thermocouples and a Resistance Temperature Detector (RTD) Fabricated Using Several Technologies

corresponding author, year	technology	slope (μV/°C)	time constant	ref
J. A. Sirs, 1961	bare wire[a]	not reported	15 ms	39
R. L. Berger, 1968	thin slab TC[b]	not reported	50 ± 5 μs (5 μm) 600 ± 25 μs (25 μm)	40, 41
M. R. Randlett, 1968	thin film TC[c]	25.9(46% of bulk)	<1 μs	42
S. Shtrikman, 1974	thin slab TC[d]	not reported	0.25 μs	43
N. E. Hager, Jr., 1985	foil TC[e]	not reported	2 s	44
J. J. Ritsko, 1987	thin film TC[f]	13.8(74% of bulk)	60 ns	45
E. Schreck, 1992	thin film TC[g]	7(33% of bulk)	0.5 μs	46
E. Schreck, 1993	thin film TC[h]	7(33% of bulk)	250 μs	47
A. Hasan, 1993	disc TC[i]	not reported	3.4 ms	48
A. Lewis, 1995	micropipette-based submicrometer TC[j]	7(95% of bulk)	<0.4 μs	28
S. T. Ro, 1996	bare wire TC[k]	not reported	86 ms	49
E. M. Castro, 2000	thin film TC[l]	53(96% of bulk)	not reported	50
J. P. Prenel, 2000	thin film TC[m]	4.4 ± 0.6(35% of bulk)	1 ± 0.1 ms	51
D. R. Buttsworth, 2001	surface junction TC[n]	not reported	<1 μs	52
D. Chu, 2003	thin film TC[o]	6−7(28−32% of bulk)	<0.4 μs	27
D. Chu, 2003	thin film TC[p]	2.9 ± 0.6(14% of bulk)	0.3 ± 0.03 μs	53
J. R. Ho, 2004	thin film TC[q]	30(76% of bulk)	5 ms	54
M. Tagawa, 2005	cold wire[r]	not applicable	11 μs	38
B. Revaz, 2005	thin film TC[s]	6(38% of bulk)	200 μs	55
E. Bordatchev, 2005	surface-wire TC with graphite film[t]	37−44(74−88% of bulk)	5−6 ns	56
X. Li, 2006	embedded thin film TC[u]	41.4(96% of bulk)	46 ns	57
X. Li, 2006	thin film TC[v]	28(68% of bulk)	40 ns	58
M. Cattani, 2006	thin film TC[w]	3.62(56% of bulk)	not reported	59
this work	sub-μm wire−thin film	19.89 ± 0.58(95% of bulk)	0.89 ± 0.19 μs	
	sub-μm wire	20.04 ± 1.22(95% of bulk)	4.53 ± 0.05 μs	
	etched sub-μm wire	20.52 ± 1.04(98% of bulk)	0.9 ± 0.2 μs	

[a] A thermocouple composed of 46 swg wires of Cu and Eureka on a silicon oxide surface. The response time was investigated by discharging a condenser, discharge lasting <1 ms. The temperature change was 2 °C. The time constant was the time it took to decay to 10% of the maximum signal. [b] A thermocouple composed of a thin slab (5−25 μm thick) of Chromel and Alumel. The slab was formed from 25 μm wires welded together and ground to the required dimensions. The response time was investigated by immersing the junction in ethanol and measuring the time it takes to reach 50% of the maximum temperature change. [c] A TFTC composed of a copper film of thickness 1250 Å and a constant film of variable thickness, down to 240 Å deposited on a glass slide. The response time was investigated with a Nd:YAG laser, 12 W/cm^2, and 1 ms pulse width. [d] A thermocouple composed of Co and Cu nanowires 100 nm in width prepared by photolithography coupled with focused ion beam (FIB). The response time was investigated with a Nd:YAG laser, 0.2 mJ, and 200 ns pulse width. The time constant was defined as the time it takes to go from 10 to 90% of the maximum signal. [e] A thermocouple composed of 0.0013 cm thick foil of Cu and Constantan and covered with 0.0089 cm of Teflon. The response time was investigated by pressing the thermocouple onto an Al plate that was 56 °C hotter than the ambient temperature. The time constant was defined as the time it took to reach 50% of the maximum temperature change. [f] A thermocouple composed a 0.51 μm thick Pt film and 0.29 μm thick Ir film on alumina. The junction was coated with 1.72 μm of alumina and 1.12 μm of Al was deposited on top of the alumina coating. A Nd:YAG laser, 1.06 μm, 10 ns pulse width, and a 10 Hz repetition rate were used to investigate the time response. The time constant is given as the time at full-width half-maximum. [g] A thermocouple composed of a 4 μm thick film of Ni and a 200 nm thick film of Au on 20 μm of alumina on a TiC−Al_2O_3 ceramic composite (a magnetic recording slider). A 30 μm thick film of alumina was evaporated on top of the thermocouple. The response time was investigated with a 500 ns laser pulse. [h] A thermocouple composed of a 4 μm thick, 80 nm wide Ni film, and a 200 nm thick Au film embedded in alumina. A 50 μs heat pulse from a resistive heater was used to investigate the time response. The time constant is taken as the time it takes to reach 90% of the signal in air. [i] A thermocouple composed of a 2.5 μm thick disk-shaped junction formed from 0.02 mm diameter Chromel and Alumel wires. The thermocouple was placed in a constant flow of Refrigerant-113 that was heated by an argon ion laser with a power of 6 mW. The response time was taken as the time it took the thermocouple to follow 63% of the maximum signal change. [j] A thermocouple composed of a Au-coated glass micropipette with a Pt core. The tip diameter was 1 μm. A Q-switched Nd:YAG laser, 1.064 μm, 300 ns pulse width, 1 mJ, and 100 Hz repetition rate were used to investigate the time response. The time constant is given as the rate of cooling of the TC after the laser pulse in air. [k] A thermocouple composed of 25 μm thick Cu and Constantan wires fused to form a junction. The response time was investigated by applying a 14 V dc pulse for 20 ms. The time constant is defined as the time it takes for the signal to decay by 36.8%. [l] A thermocouple composed of a thin film of Fe and Constantan. The thickness of the Fe thin film was varied. The time response was not investigated. [m] A thermocouple composed of >200 nm thick Au and Pd film on glass. An Ar ion laser, 514 nm, 52 mW, and a 200 Hz square wave function generator were used to investigate the time response. The time constant is taken as the time it takes to reach 95% of the output signal in air. [n] A thermocouple composed of a 3.25 mm hollow Alumel wire with a 0.8 mm Chromel wire inserted. The wires were insulated from each other along their length. The junction was formed by scratching the exposed surface to bridge the insulation. The response time was investigated with the thermocouple mounted inside a shock tube filled with 94.3 kPa of air at 21.6 °C. The thermocouple experienced a temperature change as the shock wave passed it. The time constant was defined as the time it took to go from 10 to 90% of the signal. [o] A thermocouple composed of a 120 nm thick Au and a 50 nm thick Ni film on SiO_2. The thermocouple was covered with a 300 nm thick layer of PMMA. A Nd:YAG, 10 ns pulse width, was used to investigate the response time. The time constant was defined as the time it takes to go from 10 to 90% of the maximum signal. [p] A thermocouple composed of a 50 nm thick Au film and a 30 nm thick Ni film on silicon oxide. The thermocouple is covered by PMMA. A Nd:YAG laser with a 10 ns pulse width was used to investigate the time response. The time constant is given as the time it takes to go from 10 to 90% of the signal in air. [q] A thermocouple composed of 1 μm thick sputtered films of Chromel and Alumel on an ultrasonic wire bond pad. The response time was investigated during the wire bonding process, with ultrasonic power set to 40 W, vibration frequency set to 60 Hz, and vibration time set to 20 ms. The time constant was defined as the time it took to go from 10 to 90% of the maximum signal. [r] A RTD consisting of a suspended 0.63 μm diameter platinum wire. The time constant in this case is taken to be the $1/f$ evaluated at the frequency at which the temperature gain was attenuated by 0.95. [s] A thermocouple composed of a 200 nm Au film and a 500 nm Pd film on a polyimide-coated steel foil. Response time was investigated using a 104 μs, 116 W discharge from an electron discharge machine (EDM). The time constant is taken as the time it took to go from 10 to 90% of the signal in air. [t] A thermocouple composed of a 0.25 mm diameter Constantan wire inserted through 0.57 mm diameter holes drilled into a steel plate. The Constantan wire was held in place with ceramic cement. A graphite film (0.1−2 μm thick) was used to contact the two materials. A Nd:YAG laser, 0.31 μJ, and 15 ns pulse width were used to investigate the time response. The time constant was given as the time it took to go from 10 to 90% of the signal. [u] A thermocouple composed of 100 nm thick thin film of Chromel and 100 nm thick thin film of Alumel on 0.75 μm alumina on top of 1.0 μm silicon nitride. The junction was also covered with 0.75 μm alumina and 1.0 μm silicon nitride. The insulator-embedded thermocouple was further embedded in Ni. The response time was investigated with a Nd:YAG laser, 355 nm, 10 ns pulse width, and 20 Hz repetition rate. The time constant was defined as time it took to go from 10 to 90% of the signal. [v] A thermocouple composed of a 45 nm Alumel film and a 30 nm Chromel film on an insulating layer composed of Al_2O_3 and Si_xN_y and embedded in Ni. A Q-switched Nd:YAG laser, 355 nm, 10 ns pulse width, and a 20 Hz repetition rate were used to investigate the time response. The time constant is given as the time is takes to go from 10 to 90% of the signal in air. [w] A thermocouple composed of 141 nm thick thin film of Au and a thin film of Pt (thickness 2.2−166 nm) on a glass slide. The response time was not investigated.

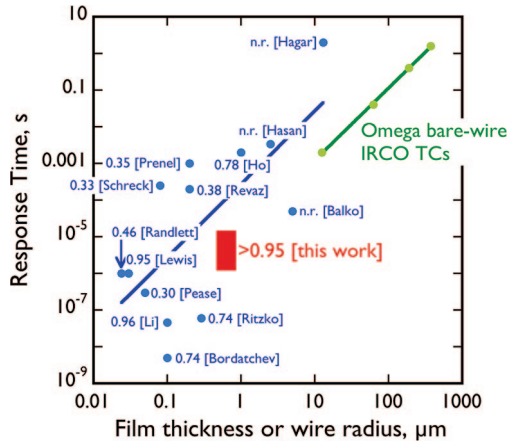

Figure 1. Plot of the response time versus the film thickness (for TFTCs) or junction radius (for TCs). Shown in green are data for iron−constantan (type J) bare-wire TCs available commercially from Omega Inc. Blue data points show response times for TFTCs and hybrid wire-film thermocouples. Next to each data point is the decimal fraction of the expected bulk sensitivity, S_{bulk}, that was retained by the device (S/S_{bulk}). The solid blue line is a least-squares fit of a polynomial to the blue data points, yielding an exponent of 1.997 and a correlation coefficient of 0.988. The red rectangle encompasses the data reported in this paper.

Thin film thermocouples derived from metal films less than 100 nm in thickness have produced response times in the microsecond range (Table 1 and Figure 1) but the Seebeck coefficient governing the sensitivity of TFTCs is degraded as the metal film thickness approaches the mean free path of electrons, l, an effect first reported in 1966.[24] For most metals of interest, l is in the range from 20 to 80 nm. In fact, for metal films with thicknesses $t \gg l$, theory predicts that the depression in sensitivity, $S_{bulk} - S_{TFTC}$, is proportional to $1/t$.[25] This loss of sensitivity can be significant: TFTCs fabricated from 50 and 30 nm thin films of Au and Ni[26,27] produced a sensitivity of 2.9 μV/°C—a depression of 86% from the bulk value of 21.4 μV/°C. In other cases (Table 1), the depression in sensitivity was in the range from 10 to 70%. A recently described innovation, called a micropipette TC, by one research group[28] is the coupling of a micrometer-scale wire with an evaporated metal film. Two research groups[28,29] have probed similar designs independently and one has achieved response times down to 5 ns[29] but the reliance of this design on an ultrathin metal film of sub-100 nm thickness ensures that sensitivities are significantly below bulk values just as seen for other TFTCs. With just one exception,[30] the literature supports the conclusion that, for TFTCs, even those employing innovative architectures, temperature sensitivity must be sacrificed to obtain response times below 1 μs.

In principle, this "catch 22" can be circumvented by using purely wire-based thermocouples that have a heat capacity proportional to (radius)^2 of the wires. In a recent communication,[31] we described a new method for fabricating wire-based silver/nickel TCs with diameters in the 500−800 nm range, much larger than l (≈50 nm). The response time for ensembles of these "submicrometer" TCs were in the microsecond range while the sensitivity of these junctions was indistinguishable from bulk.[31] In this full paper, we provide a more complete disclosure of our methods for TC fabrication, we explore the properties of these devices in greater depth, and we compare them to hybrid wire−thin film TCs.

II. Materials and Experimental Procedures

II.a. Fabrication of Submicrometer Wire−Thin Film Thermocouples (SMTF). The procedure, shown schematically in Figure 2a, involved the electrodeposition of silver nanowires onto a graphite electrode, the transfer of these nanowires to a cyanoacrylate-coated glass slide, and the evaporation of a nickel film over part of these transferred nanowires. Submicrometer silver wires were electrodeposited onto the step edges present on a freshly cleaved surface of a (0001) highly oriented pyrolytic graphite (HOPG) crystal (GE Advanced Ceramics ZYB grade) using the electrochemical step edge decoration (ESED) method described previously.[32−34] In step one, silver wires with a diameter of 500−800 nm were electrodeposited from an aqueous (Millipore, $\rho = 18.2$ MΩ-cm) solution containing 1 mM Ag_2SO_4 (Sigma Aldrich, 99.999%), 1 mM saccharin (Alfa Aesar, 98+%), 0.1 M Na_2SO_4 (Fisher, enzyme grade), and H_2SO_4 (JT Baker Ultratex II) to adjust the pH to 1.0. During this wire deposition process (and all of the subsequent wire depositions described below), the HOPG electrode was held within a Teflon holder in which an O-ring presented to the plating solution a circular 3 mm diameter region of the HOPG basal plane surface. The potential program employed for silver wire growth was the following: +1.1 V for 5 s, −0.8 V for 100 ms, and −0.18 V for 900 s, all potentials referenced to a Ag wire. In step 2, these silver wires were transferred from the HOPG surface to a glass microscope slide by placing a drop of cyanoacrylate (Satellite City Special T) onto the HOPG surface where nanowires had been deposited and then pressing this surface onto the microscope slide. After the cyanoacrylate was allowed to harden for 12 h, the HOPG was removed from the glass using a razor blade, leaving the silver wires embedded in an ≈1 cm diameter cyanoacrylate disk. In step 3, a shadow mask was placed over half of the silver wires to isolate a rectangular area (6 mm × 11 mm) for the evaporation of a nickel (ESPI, catalog no. K36021, purity 4N5) metal thin ($t = 40$ nm) film. Finally, electrical contacts to the silver wires and nickel thin film were formed using conductive silver paste (Ted Pella Cat.

(24) Marshall, R.; Atlas, L.; Putner, T. *Rev. Sci. Instrum.* **1966**, *43*, 144.
(25) Cattani, M.; Salvadori, M. C.; Vaz, A. R.; Teixeira, F. S. *J. Appl. Phys.* **2006**, 100.
(26) Chu, D.; Bilir, D. T.; Pease, R. F. W.; Goodson, K. E. Thin film nano thermocouple sensors for applications in laser and electron beam irradiation, *Transducers '03, International Conference on Solid-State Sensors, Actuators and Microsystems, Digest of Technical Papers, 12th*, Boston, MA, June 8–12, 2003 **2003**; *2*, 1112–1115.
(27) Chu, D.; Wong, W.-K.; Goodson, K. E.; Pease, R. F. W. *J. Vac. Sci. Technol. B* **2003**, *21*, 2985.
(28) Fish, G.; Bouevitch, O.; Kokotov, S.; Lieberman, K.; Palanker, D.; Turovets, I.; Lewis, A. *Rev. Sci. Instrum.* **1995**, *66*, 3300.
(29) Heichal, Y.; Chandra, S.; Bordatchev, E. *Exp. Therm. Fluid Sci.* **2005**, *30*, 153.
(30) Datta, A.; Choi, H.; Li, X. *J. Electrochem. Soc.* **2006**, *153*, H89.
(31) Bourg, M. E.; van der Veer, W. E.; Güell, A.; Penner, R. M. *Nano Lett.* **2007**, *7*, 3208.
(32) Walter, E. C.; Murray, B. J.; Favier, F.; Kaltenpoth, G.; Grunze, M.; Penner, R. M. *J.Phys. Chem. B* **2002**, *106*, 11407.
(33) Walter, E. C.; Zach, M. P.; Favier, F.; Murray, B. J.; Inazu, K.; Hemminger, J. C.; Penner, R. M. *ChemPhysChem* **2003**, *4*, 131.
(34) Penner, R. M. *J. Phys. Chem. B* **2002**, *106*, 3339.

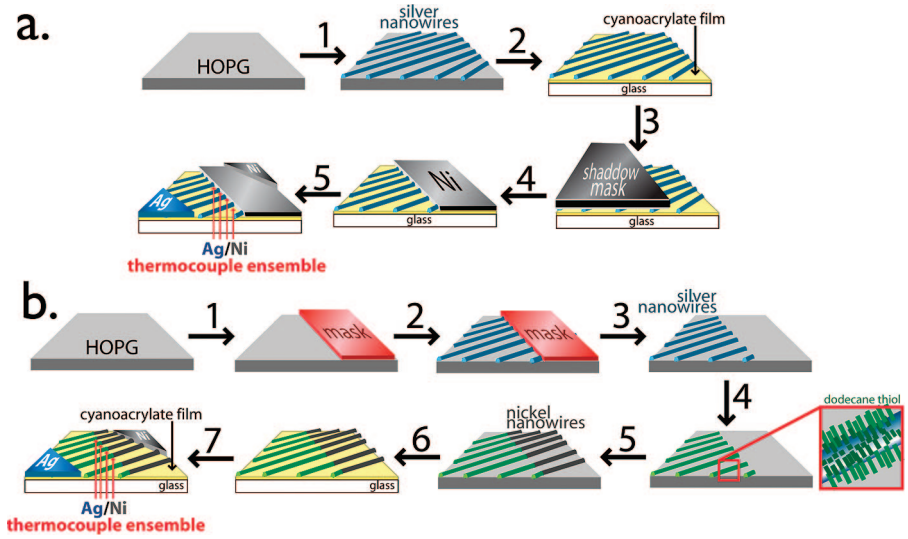

Figure 2. (a) Fabrication scheme for submicrometer wire−thin film thermocouples (SMTF TCs). (b) Fabrication scheme for submicrometer wire thermocouples (SMTCs).

16032) and conductive nickel print (MG Chemicals Cat. 840-20 g), respectively. Silver (diameter = 0.5 mm, Alfa Aesar, 99.9985%) and Ni (diameter = 0.5 mm, Scientific Instrument Services, 98+%) extension wires were secured to the painted contacts using epoxy (Loctite Hysol 1C).

Submicron wire-thin film thermocouples were also prepared using nickel wires and an evaporated silver film. In this case, nickel wires were electrodeposited from an aqueous solution containing 5 mM $NiCl_2 \cdot 6H_2O$ (Acros Organics, 99.9999%), 3 mM $NiSO_4 \cdot 6H_2O$ (Aldrich, 99%), 0.01 M H_3BO_3 (Acros Organics, 99.99%), and 0.1 M Na_2SO_4 (Fisher, enzyme grade) using the following potential program: −1 V for 5 ms, −0.7 V for 600 s versus a saturated calomel reference electrode. The nickel wires were transferred to glass as before and a 40 nm thick silver film (Alfa Aesar, catalog no. 11469, purity 99.9985%) was evaporated. Electrical contacts were attached as before. Our success rate for obtaining functioning SMTF TCs using this approach was 90%, start to finish.

II.b. Fabrication of Submicrometer Wire Thermocouples (SMTCs). The process flow shown in Figure 2b was used to produce an ensemble of 2–20 TCs consisting of end-butted silver and nickel wires of similar diameters in the 500−800 nm range. To achieve this result, half of the deposition area on the HOPG substrate was first masked using Crystalbond, an acetone-soluble masking agent (Ted Pella, Cat. 821-1) by melting it directly onto the HOPG surface heated on a hot plate (Figure 2b, step 1). Then in step 2, silver wires with a diameter of 500−800 nm were electrodeposited on unmasked regions of the HOPG surface as described above. The Crystalbond mask was then completely removed by exhaustively rinsing the surface in acetone (EMD, HPLC grade) five times in succession, followed by rinses in HPLC-grade methanol, isopropanol, and water (Millipore, $\rho = 18.2$ MΩ cm). In step 4, the silver wires were coated with a self-assembled monolayer of 1-decanethiol (TCI America, 98%) from a 2 mM solution in ethanol (Gold Shield, 200 proof). This effectively insulated these wires from contact with the electrolyte solution, ensuring that nickel was not deposited atop them in the next step. In step 5, nickel wire segments were electrodeposited, as described above, on regions of the HOPG from which the Crystalbond mask had been removed. Finally, in step 6, the Ag/Ni SMTCs produced in steps 1−5 were transferred from the graphite surface onto a glass microscope slide using cyanoacrylate adhesive and electrical contacts were added as described above.

A subset of the SMTCs were subjected to an additional processing step that involved etching of the silver wires after step 2 to produce etched submicrometer wire thermocouples (ESMTCs). Etching involved the application of 1 μA of anodic current for 1000 s immediately after silver electrodeposition in step 2. As described below, etching significantly affected the performance of SMTCs. Our success rate for obtaining functioning SMTCs and ESMTCs using this approach was 80%, start to finish, with virtually all failures caused by faulty electrical contacts.

II.c. Scanning Electron Microscopy. Scanning electron microscopy (SEM) was carried out on uncoated samples using a Philips FEG-30XL microscope with energy-dispersive X-ray (EDX) analysis capabilities. For all devices, both sides of the junction were electrically grounded using the silver and nickel extension wires. Submicrometer wire (SMTC) and etched submicrometer wire (ESMTC) thermocouples were imaged prior to removal from the HOPG surface. An accelerating voltage of 10 kV was used for SEM imaging, whereas for energy-dispersive X-ray microanalysis (EDX), 20 kV was used.

II.d. Thermocouple Calibration. Thermocouples were calibrated over the temperature range from 20 to 110 °C using an apparatus that consisted of a resistive heating element (DALE RH 50, 50 W, 22 Ω) mounted to a 0.5 in. thick aluminum plate. A standard thermocouple (type J (Omega, IRCO-010) mounted on a glass slide in cyanoacrylate adhesive) was located on one side of this heating element and on the other, symmetrically, was mounted the sample to be calibrated. A programmable power supply (Agilent, E3643A) powered the heating element. The temperature of the reference junction of the submicrometer wire-based

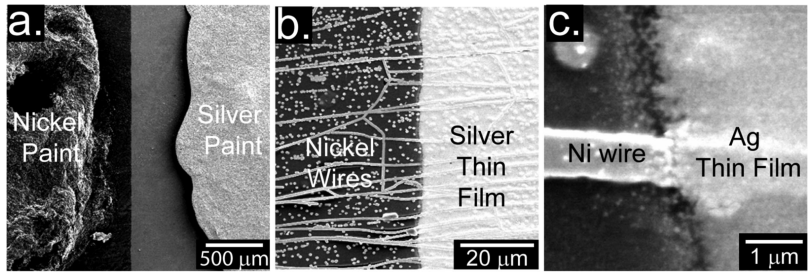

Figure 3. (a) Low-magnification scanning electron microscope image of a submicrometer wire−thin film thermocouple. (b) SEM image of a SMTF TC revealing multiple junctions between the Ni wires and the Ag film. (c) High-magnification SEM image of one of the Ni wire−Ag film junctions shown in (b).

thermocouple was monitored with a type J thermocouple (Omega, IRCO-010) and the outputs of both type J thermocouples were measured with Keithley 2000 digital multimeters equipped with Model 2001-TCSCAN cards. A third Keithley 2000 digital multimeter measured the output voltage of the submicrometer wire-based thermocouple. Heating, cooling, and data acquisition from this apparatus was coordinated using National Instruments LabView. Heating and cooling rates were 0.018 °C/s and 0.016 °C/s, respectively.

II.e. Response Time Measurements. Two methods were employed for characterizing the response time of TCs: *Method 1*. The output from a continuous wave argon ion laser (Coherent Innova 90, $\lambda_{ex} = 514$ nm, 350 mW) was mechanically chopped (Stanford Research Systems, SRS42) and directed onto the TC at normal incidence. The chopping frequency was varied from 20 Hz to 3.9 kHz. The signal from the thermocouple was amplified with a voltage preamplifier (Stanford Research Systems, SR560) and recorded on a digital storage oscilloscope (Tektronix, TDS 1012). The peak-to-peak amplitude was normalized to the signal amplitude at 20 Hz for each thermocouple. The response time was defined as the $1/f$ where f was the frequency at which the normalized output, $V_{TC}/V_{TC,\ 20\ Hz} = 0.05$. *Method 2*: More rapid heating was produced using either of two frequency-doubled ($\lambda_{ex} = 532$ nm) Nd:YAG lasers—the first was a Continuum Surelite 1 that had a beam diameter of 8 mm, a pulse duration of 7 ns, and a peak power density at the TC of 0.57 MW/cm^2. The second, a Quantel Brilliant, had a pulse duration of 4 ns, a beam diameter of 6 mm, and a peak power density at the TC that could be varied from 0.236 to 8.14 MW/cm^2. The current response of each TC was measured using a trans-impedance amplifier (National LMH6624) in conjunction with a digital storage oscilloscope (Tektronix, TDS 1012).

III. Results and Discussion

III.A. Device Fabrication and Characterization by Scanning Electron Microscopy. Silver/nickel thermocouples were targeted in this study because these two metal are readily electrodeposited as nanowires using the ESED method, both metals resist oxidation in air, and the predicted Seebeck coefficient for the Ag/Ni junction is reasonably high at 21 μV/°C. Submicrometer wire−thin film thermocouples (SMTF TCs) were prepared by evaporating a 40 nm silver film on approximately half of the nickel wires that were embedded in the cyanoacrylate adhesive on the glass slide

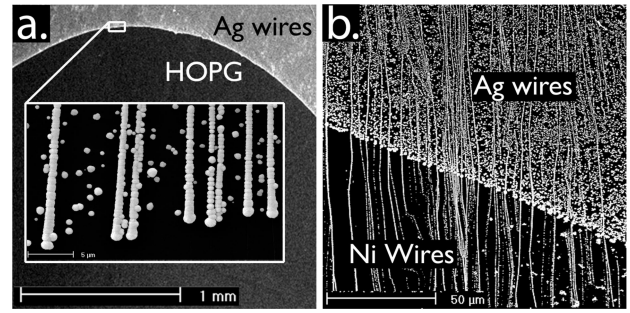

Figure 4. (a) Scanning electron microscope (SEM) image of the silver submicrometer wires on HOPG after removal of the CrystalBond. (b) SEM image of several junctions formed between the silver and nickel wires on HOPG.

as shown schematically in Figure 2a. Scanning electron microscope images of the interface between the metal film and the nanowires (Figure 3b) show 0.5−2 junctions per 1.0 μm of interface. SEM images of a device are shown in Figure 3. The painted contacts (Figure 3a) encompassed several thousand junctions, on average, arranged electrically in parallel. This fabrication method had a success rate—defined as the fraction of SMTCs that reliably measured temperature (see below)—of 90% from start to finish with nearly all failures resulting from detachment of the painted contacts from the thin film surface and/or detachment of the extension wires from the painted contacts.

The fabrication of thermocouples consisting of silver/nickel wires (SMTCs) was more complex, involving seven operations as follows (Figure 2b): (1) masking half of the exposed region of a freshly cleaved HOPG surface with CrystalBond by physically transferring a small droplet of this material onto the heated HOPG surface, (2) electrodeposition of silver wires on unmasked regions of the HOPG surface using the ESED method (Figure 4a), (3) removal of the CrystalBond mask by exhaustive extraction in acetone (see above), (4) coating of the silver wires with a monolayer of decanethiol from an ethanolic solution, (5) electrodeposition of nickel wires using the ESED method at the previously masked region of the HOPG surface (Figure 4b), (6) transfer of the resulting bimetallic submicrometer wires from the HOPG surface to a glass microscope slide with cyanoacrylate, and, (7) the application of electrical contacts to the transferred junctions. It is worth adding that the oxidation of the nickel side of the TC, in particular, has the potential to interfere with the establishment of an intimate electrical contact with the silver wires but this problem is apparently circumvented by electrodepositing the nickel wires after the silver wires,

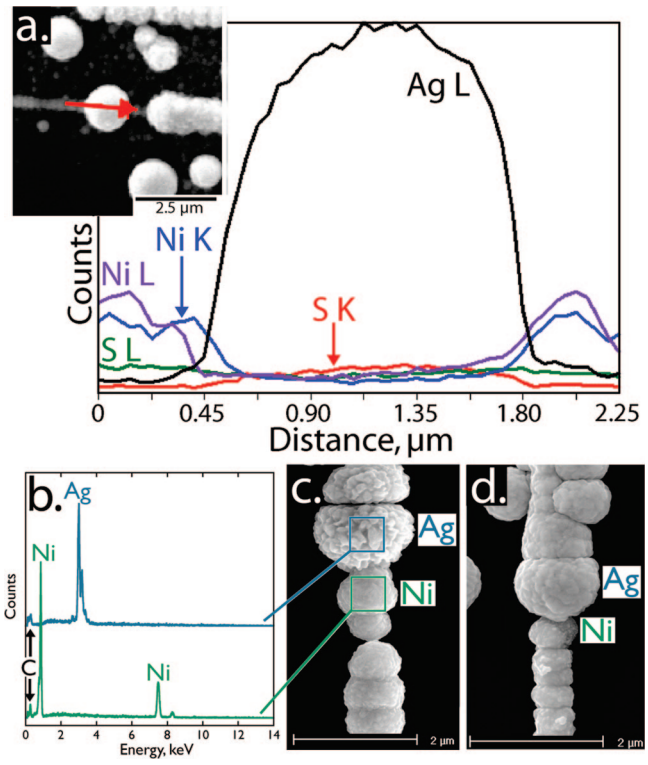

Figure 5. (a) X-ray line scan along a Ni wire that contains a silver particle. (b) Energy-dispersive X-ray analysis of the silver and nickel wires immediately adjacent to the junction shown in (c). (c) High-magnification SEM image of a single junction formed between an etched silver wire and nickel wire. (d) High-magnification SEM image of a junction formed between a silver wire and a nickel wire.

thereby ensuring that elemental nickel is formed directly in contact with the pre-existing silver wires.

The purpose of step 4—the coating of silver wires with decanethiol—is to prevent the electrodeposition of nickel on these wires in step 5, limiting it instead to the clean step edges revealed by the removal of the CrystalBond mask in step 3. The efficacy of this monolayer in suppressing the electrodeposition of nickel on the silver wires is demonstrated by the data shown in Figure 5. After the deposition of nickel (narrow wire in Figure 5a inset), X-ray fluorescence (EDX) line scans across a silver particle reveal no nickel (blue and purple traces) and a barely detectable sulfur signal (red and green traces). EDX spectra of the two sides of a ESMTC junction (Figure 5b,c) also show that the silver side of the junction is not contaminated by nickel while, not unexpectedly, the nickel side is free from silver.

One elaboration to this fabrication procedure for SMTCs was investigated: We electrochemically etched the silver wires immediately after their deposition in step 2 of this procedure by applying an anodic current of 1 μA for 1000 s.[35] Our objective in carrying out this etching procedure was to reduce the diameter of the silver wires but this etching process acted preferentially at interparticle boundaries along the axis of each silver wire, producing deep crevices at these boundaries without reducing the overall diameter significantly. The roughness of the silver surfaces was also increased by this etching, as seen in the SEM images of Figure 5c (etched) and 5d (not etched). We demonstrate below that these etched submicrometer wire thermocouples (or ESMTCs) showed significantly faster thermal response behavior, suggesting that these crevices thermally decoupled the junction from the silver connection, thereby reducing its thermal mass. For purely practical reasons, wires of just one metal (either silver or nickel) could be subjected to this etching process. We selected silver because its higher thermal conductivity (430 W m^{-1} K^{-1} versus 91 W m^{-1} K^{-1} for nickel) means that stronger axial thermal coupling[36] on the silver side of this junction makes a larger contribution to the total thermal mass of the junction than axial coupling on the nickel side. The success rate for fabrication of SMTCs and ESMTCs was 80% start to finish, with nearly all failures resulting from the detachment of the extension wires from the painted contacts.

III.B. Calibration, Hysteresis, and Stability. A primary objective of exploring submicrometer wires for thermocouples is to reduce or eliminate the depression in the Seebeck coefficient, S, that has been observed for TCs based upon ultrathin metal films (Figure 1 and Table 1). This depression in S is observed when the thickness of one or both metal films approaches the electron mean free path in these metals.[25] We measured the effective Seebeck coefficient for all three types of junctions (SMTC, SMTF, and ESMTC) in the temperature range from ambient to 110 °C. This upper limit is dictated by the decomposition temperature of the cyanoacrylate employed for these devices which was ≈150 °C. Output voltage, V_{TC}, versus temperature calibration plots are shown for 33 SMTF TCs in Figure 6a. The lowest and highest slopes recorded for these devices, shown by the green and yellow traces, correspond to Seebeck coefficients of 15.7 to 20.4 μV/°C, respectively. These limits represent 75 to 97% of the bulk value for a Ag/Ni thermocouple (S_{bulk} = 21 μV/°C). The average for these 33 devices was 19.9 ± 0.6 μV/°C. These high values for S are somewhat surprising because the thickness of the silver films in these devices (40 nm) was somewhat smaller than the ≈50 nm mean free path (mfp) for electrons in polycrystalline silver,[37] but this conclusion is robust as it is based upon measurements on 33 different devices.

The analogous calibration results for 17 SMTCs and 12 ESMTCs are shown in Figures 6b and 6c, respectively. The mean Seebeck coefficients for these two sets of devices were 20 ± 1 μV/°C, for SMTCs, and 21 ± 1 μV/°C for ESMTCs—statistically indistinguishable from the bulk S value. The minimum Seebeck coefficient seen in either data set was 90% of the bulk. The process depicted in Figure 2b effectively produces electrochemically butt-welded Ag/Ni 0.8−1.1 μm diameter wires, dimensions much greater than electron mfp in these metals, so there is no reason to expect a depressed Seebeck coefficient and these data confirm that none is observed.

We also looked for the presence of hysterisis in heating/cooling curves that could signal mechanical deformations of the junctions in these devices caused by thermal expan-

(35) Thompson, M. A.; Menke, E. J.; Martens, C. C.; Penner, R. M. *J. Phys. Chem. B* **2006**, *110*, 36.

(36) Fralick, G. C.; Forney, L. J. *Rev. Sci. Instrum.* **1993**, *64*, 3236.

(37) Qin, X. Y.; Zhang, W.; Zhang, L. D.; Jiang, L. D.; Liu, X. J.; Jin, D. *Phys. Rev. B* **1997**, *56*, 10596.

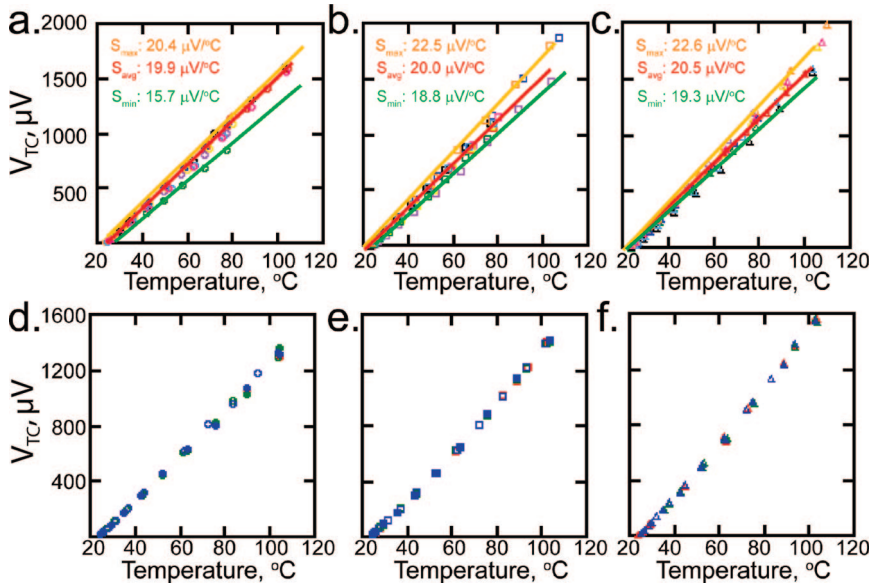

Figure 6. (a) Heating calibration for 33 Ag/Ni SMTF TCs. The mean sensitivity measured was 19.9 ± 0.58 μV/°C and it ranged from a minimum of 15.7 to 20.4 μV/°C. (b) Heating calibration for 17 Ag/Ni SMTCs. The mean sensitivity measured was 20.0 ± 1.2 μV/°C and it ranged from a minimum of 18.8 to 22.5 μV/°C. (c) Heating calibration for 12 Ag/Ni ESMTCs. The mean sensitivity measured was 20.5 ± 1.0 μV/°C and it ranged from a minimum of 19.3 to 22.6 μV/°C. (d) Three heating and cooling curves for a SMTF TC revealing a modest amount of hysterisis at the higher temperature region. (e) Three heating and cooling curves for a SMTC showing the absence of hysterisis. (f) Three heating and cooling curves for an ESMTC revealing the absence of hysterisis. Heating and cooling rates were 0.018 °C/s and 0.016 °C/s, respectively.

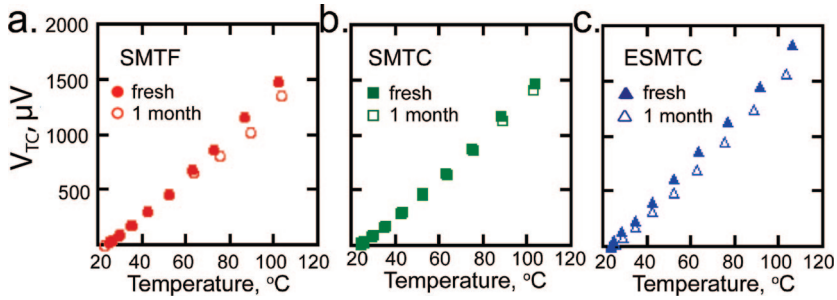

Figure 7. (a) Heating curves for a single SMTF TC that is "fresh" and for the same SMTF TC after storage for 1 month in laboratory air. (b) Heating curves for a single SMTC that is "fresh" and for the same SMTC after storage for 1 month in laboratory air. (c) Heating curves for a single ESMTC that is "fresh" and for the same ESMTC after storage for 1 month in laboratory air. Heating and cooling rates were 0.018 °C/s and 0.016 °C/s, respectively.

sion/contraction. In these experiments, heating and cooling rates were 0.018 °C s^{-1} and 0.016 °C s^{-1}, respectively. Disparities in the Seebeck coefficient were, at most, 0.1 μV/°C in these trials for any of the three device types. A small number of devices of each type were also subjected to a more rigorous test that involved cycling the temperature between 20 and 110 °C for 24 consecutive hours (Table 2). The three types of devices performed nearly identically in this test, producing S_{Ave} values of 18.3−19.7 μV/°C with standard deviations of less than 0.6 μV/°C.

Longer term stability, on the time scale of weeks to months, is a potential issue for these devices as oxidation of the silver and nickel components gradually occurs. Of course, the stability of a thermocouple depends upon the measuring environment, i.e., temperature, oxidative versus reductive atmosphere, and mechanical strain/stress. The stability of submicrometer wire-based thermocouples was assessed 1 month after initial calibration experiments with storage in a laboratory air ambient at 20−25 °C and nominal ≈55% relative humidity (Figure 7 and Table 2). All three types of TCs showed reduced S_{Ave} values over this time period with the largest decreases (−13%) seen for SMTF TCs and ESMTCs (−10%). Seebeck coefficients for SMTCS were smaller by just 4%.

Table 2. Seebeck Coefficients for Thermocouples after Exposure to Laboratory Air of 24 h and 1 month

24 h device	S_{Ave} (μV/°C)[a]
SMTF	19.7 ± 0.6
SMTC	18.3 ± 0.3
ESMTC	19.5 ± 0.2

1 month device	S_{Ave} (μV/°C)[b]	ΔS_{Ave}, %[c]
SMTF	16.4 ± 0.4	−13%
SMTC	17.6 ± 0.1	−4%
ESMTC	19.5 ± 0.2	−10%

[a] These values represent the mean and standard deviation of the Seebeck coefficient seen for continuous temperature cycling of a device for 24 h in laboratory air. [b] These values represent the mean and standard deviation of the Seebeck coefficient measured for devices that were exposed to laboratory air for approximately 1 month. The initial Seebeck coefficients in all cases were in the 18−22 μV/°C range seen for freshly prepared devices. [c] Change in the Seebeck coefficient as a percentage of the initially measured value for the fresh device.

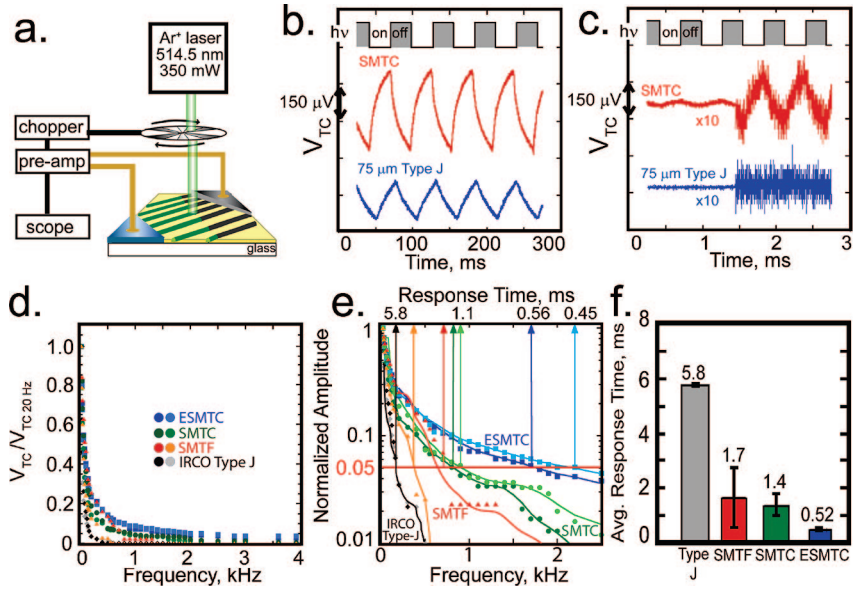

Figure 8. Summary of steady-state response time measurements: (a) Schematic diagram of the response time measurement system. A CW Ar ion laser (λ_{ex} = 514 nm, beam diameter = 2 mm, power = 350 mW) was used to heat the measuring junction of the thermocouple. A mechanical chopper was used to modulate the pulse duration. The thermocouple output, V_{TC}, was amplified and the transient was recorded on an oscilloscope. (b) V_{TC} versus time traces at a chopping frequency of 20 Hz for a SMTC and a 75 μm type J thermocouple. (c) V_{TC} versus time transients for the same TCs shown in (b), but at a chopping frequency of 1.8 kHz. (d) Plot of the V_{TC} normalized to V_{TC} at 20 Hz versus the chopping frequency for a 75 and 125 μm type J TC, Ag/Ni SMTF TCs, Ag/Ni SMTCs, and Ag/Ni ESMTCs. (e) Log-normal plot of the same data shown in (d). (f) Bar graph revealing the average response times for type J TCs, SMTF TCs, SMTCs, and ESMTCs. The response time was defined as the time ($1/f$) when the signal was attenuated to $V_{TC}/V_{TC,\ 20\ Hz} = 0.05$.

III.C. Temporal Response Properties. To our knowledge, there is no standard method for assessing the temporal response properties of TCs. This means that detailed, unequivocal comparisons with literature results are not possible. We nevertheless measured the temporal properties of all three types of submicrometer wire-based TCs using two different laser heating methods that were similar to methods employed in other studies summarized in Table 1 and Figure 1. We included in this evaluation two commercial bare-wire thermocouples (Omega, type J, 75 and 125 μm diameters). These commercial type J TCs were mounted on glass slides with cyanoacrylate adhesive using exactly the same procedure employed for mounting of the SMTCs and ESMTCs with which they were compared.

In the first laser heating method, a chopped CW argon ion laser (350 mW (unchopped) at λ_{ex} = 514 nm) was incident on junctions of each type (Figure 8a). This illumination produced steady-state heating and cooling transients for each type of TC at chopping frequencies between 20 Hz and 3.9 kHz. Typical traces acquired in this manner at 20 and 1800 Hz (Figures 8b,c) for a SMTC and a 75 μm type J show that the voltage output of both TCs is strongly modulated at 20 Hz (Figure 8b), but the output from the type J TC is completely damped at 1.8 kHz (Figure 8c). Two metrics can be compared in this experiment: The excursion of the temperature, ΔT, at a particular frequency and the frequency response. The observed ΔT was smallest for the commercial type J TCs and progressively larger for the SMTF, SMTC, and ESMTC devices in 9 sets of experiments with different devices. For example, at a chopping frequency of 20 Hz the observed ΔT value excursions were as follows: 1.9 °C (type J), 5.9 °C (SMTF), 9.0 °C (SMTC), and 12.8 °C (ESMTC). Since the laser heating time is the same for all four devices, the observed ΔT can be related to the response times of each. Indeed, the observed response times decreased in the same order as ΔT increased. To make this comparison, we normalized the maximum output voltage at each frequency, V_{TC}, by the output observed at a reference frequency of 20 Hz, $V_{TC,\ 20\ Hz}$. The degree to which $V_{TC}/V_{TC,\ 20\ Hz}$ is attenuated as a function of frequency can be taken as an indication of the relative temporal responses of these four different types of devices. This normalized response, $V_{TC}/V_{TC,\ 20\ Hz}$, is compared for all four types of TCs as a function of chopping frequency in Figures 8d,e. In this experiment, we defined the response time to be (1/frequency) at which $V_{TC}/V_{TC,\ 20\ Hz} = 0.05$, as shown in Figure 8e for a few devices of each type. The average response times (Figure 8f) for the type J TCs, SMTF TCs, SMTCs, and ESMTCs are 5.8 ± 0.7, 1.7 ± 1, 1.4 ± 0.4, and 0.52 ± 0.06 ms, respectively.

Why are ESMTCs faster than SMTCs? A speculation based upon the known thermal properties of cylindrical wire-based TCs is the following: The time constant, τ, for TCs consisting of end-butted metal−metal junctions embedded in a uniform medium is approximated by[38]

$$\tau = \frac{\rho c r^2}{\mathrm{Nu}\lambda} \qquad (1)$$

where ρ is the mean density (kg/m^3), r is the mean radius (m), c is the effective specific heat (J/kg K), λ is the thermal conductivity (W/(m K)), and Nu is the dimensionless Nusselt number quantifying heat transfer from the thermocouple into the environment surrounding it. The effect of constrictions in the wires near the junctions is to reduce the effective value of c by impeding thermal transport along the axis of the wire on the silver side of the junction.

In the experiment just described, steady state is established and heating and cooling of the junction occurs with the same

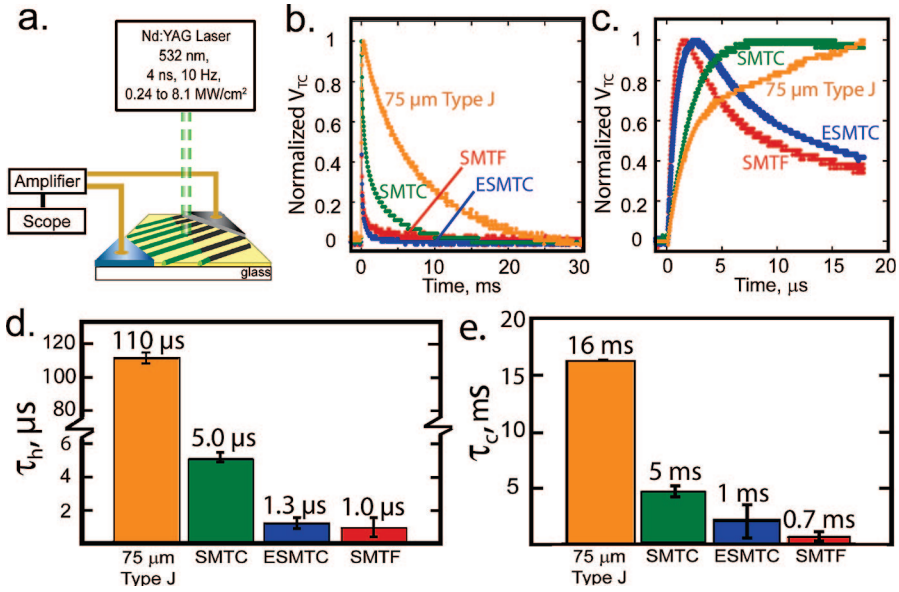

Figure 9. (a) Schematic diagram of the response time measurement system. A Quantel Brilliant Nd:YAG laser (λ_{ex} = 532 nm, beam diameter = 6 mm, pulse width = 4 ns, power density = 0.236−8.14 MW/cm^2) was used to heat the measuring junction of the thermocouple. The thermocouple output was amplified by a fast transimpedance amplifier and the output was recorded on an oscilloscope. (b) Normalized V_{TC} transients on an extended time scale for a 75 μm type J TC, a Ag/Ni SMTC, a Ag/Ni ESMTC, and a Ag/Ni SMTF TC at a peak power density of 8.1 MW/cm^2. (c) Normalized V_{TC} on a short time scale for a 75 μm type J TC, a Ag/Ni SMTC, a Ag/Ni ESMTC, and a Ag/Ni SMTF at peak power density of 8.1 MW/cm^2. (d) Average rise time for three 75 μm type J TCs, eight Ag/Ni SMTF TCs, three Ag/Ni SMTCs, and four Ag/Ni ESMTCs. The rise time is defined as the time it takes for the signal to reach 90% of the maximum signal. (e) Average decay time for three 75 μm type J TCs, eight Ag/Ni SMTF TCs, three Ag/Ni SMTCs, and four Ag/Ni ESMTCs. The decay time is defined as the time it takes for the signal to decay to 10% of the maximum V_{TC}.

apparent time constant (Figure 8b,c), namely that associated with the slower of these two processes. However, the intrinsic rates for heating and cooling are different because these are fundamentally different processes: laser heating of a cold TC junction embedded in a matrix (cyanoacrylate adhesive) and heat dissipation from a hot TC by conduction, convection, and radiation. It is possible to deconvolute these two time constants by heating these thermocouple junctions using a pulsed laser with a pulse width that is much shorter than either of the two time constants characterizing these processes.

We used either of two frequency-doubled Nd:YAG lasers with λ_{ex} = 532 nm and nominal pulse widths of 4−7 ns. Normalized output voltages ($V_{TC}/V_{TC,\,max}$) on the millisecond and microsecond time scale at a power density of 8.14 MW/cm^2 are shown in Figure 9 for all three types of submicrometer wire-based TCs and a 75 μm type J TC. We defined time constants for heating, τ_h, and cooling, τ_c, as the time required for the V_{TC} to reach 90% of its maximum (or minimum) value. Time constants for heating, τ_h, were 110 ± 7, 5.0 ± 0.3, 1.3 ± 0.4, and 1.0 ± 0.6 μs for 75 μm type J TCs, SMTC, ESMTC, and SMTF, respectively.

In principle, the amplitude of the temperature change induced by the laser pulse has the potential to affect the apparent time constants τ_h and τ_c and this can make the comparison of time constants between different experiments reported in the literature difficult. We explored the laser power dependence using a Quantel Brilliant Nd:YAG laser (λ_{ex} = 532 nm, 4 ns pulse width) capable of generating peak power densities of 8.14, 2.28, and 0.236 MW/cm^2. Unnormalized voltage transients are shown in Figure 10 a,b, revealing the effect of different power densities on an extended time scale (ms) for all three submicrometer-wire based TCs. Also observable in these plots is the difference in the maximum output voltage for the different TCs at the same peak power density. For example, the maximum output voltage for a SMTC at a peak power density of 8.14 MW/cm^2 was 36 mV, while it was only 14 and 7 mV for an ESMTC and a SMTF (Figure 10a). The average maximum output voltages at this power density were 24 ± 16, 10 ± 13, and 6 ± 2 mV for SMTC, ESMTC, and SMTF TCs, respectively. A similar effect is shown on a microsecond

(38) Tagawa, M.; Kato, K.; Ohta, Y. *Rev. Sci. Instrum.* **2005**, *76*, 094904.
(39) Sirs, J. A. *J. Sci. Instrum.* **1961**, *38*, 489.
(40) Balko, B.; Berger, R. L. *Rev. Sci. Instrum.* **1968**, *39*, 498.
(41) Balko, B.; Berger, R. L. *Biophys. J.* **1968**, *8*, A161.
(42) Chopra, K. L.; Bahl, S. K.; Randlett, M. R. *J. Appl. Phys.* **1968**, *39*, 1525.
(43) Barisaac, C.; Korn, U.; Shtrikman, S. *Appl. Phys* **1974**, *3*, 285.
(44) Hager, N. E. *Rev. Sci. Instrum.* **1985**, *56*, 421.
(45) Tong, H. M.; Arjavalingam, G.; Haynes, R. D.; Hyer, G. N.; Ritsko, J. J. *Rev. Sci. Instrum.* **1987**, *58*, 875.
(46) Schreck, E.; Fontana, R. E., Jr.; Singh, G. P. *IEEE Trans. Magn.* **1992**, *28*, 2548.
(47) Schreck, E.; Hiller, B.; Singh, G. P. *Rev. Sci. Instrum.* **1993**, *64*, 218.
(48) Beckman, P.; Roy, R. P.; Whitfield, K.; Hasan, A. *Rev. Sci. Instrum.* **1993**, *64*, 2947.
(49) Park, S. J.; Ro, S. T. *Exp. Fluids* **1996**, *21*, 380.
(50) Scarioni, L.; Castro, E. M. *J. Appl. Phys.* **2000**, *87*, 4337.
(51) Serio, B.; Nika, P.; Prenel, J. P. *Rev. Sci. Instrum.* **2000**, *71*, 4306.
(52) Buttsworth, D. R. *Exp. Therm. Fluid Sci.* **2001**, *25*, 409.
(53) Chu, D. C.; Wong, W. K.; Goodson, K. E.; Pease, R. F. W. *J. Vac. Sci. Technol. B* **2003**, *21*, 2985.
(54) Ho, J.-R.; Chen, C.-C.; Wang, C.-H. *Sens. Actuators, A* **2004**, *A111*, 188.
(55) Revaz, B.; Flükiger, R.; Carron, J.; Rappaz, A. *Sens. Actuators, A* **2005**, *118*, 238.
(56) Heichal, Y.; Chandra, S.; Bordatchev, E. *Exp. Therm. Fluid Sci.* **2005**, *30*, 153.
(57) Datta, A.; Choi, H. S.; Li, X. C. *J. Electrochem. Soc.* **2006**, *153*, H89.
(58) Zhang, X.; Choi, H.; Datta, A.; Li, X. *J. Micromech. Microeng.* **2006**, *16*, 900.
(59) Salvadori, M. C.; Vaz, A. R.; Teixeira, F. S.; Cattani, M.; Brown, I. G. *Appl. Phys. Lett.* **2006**, *88*, 133106/1.

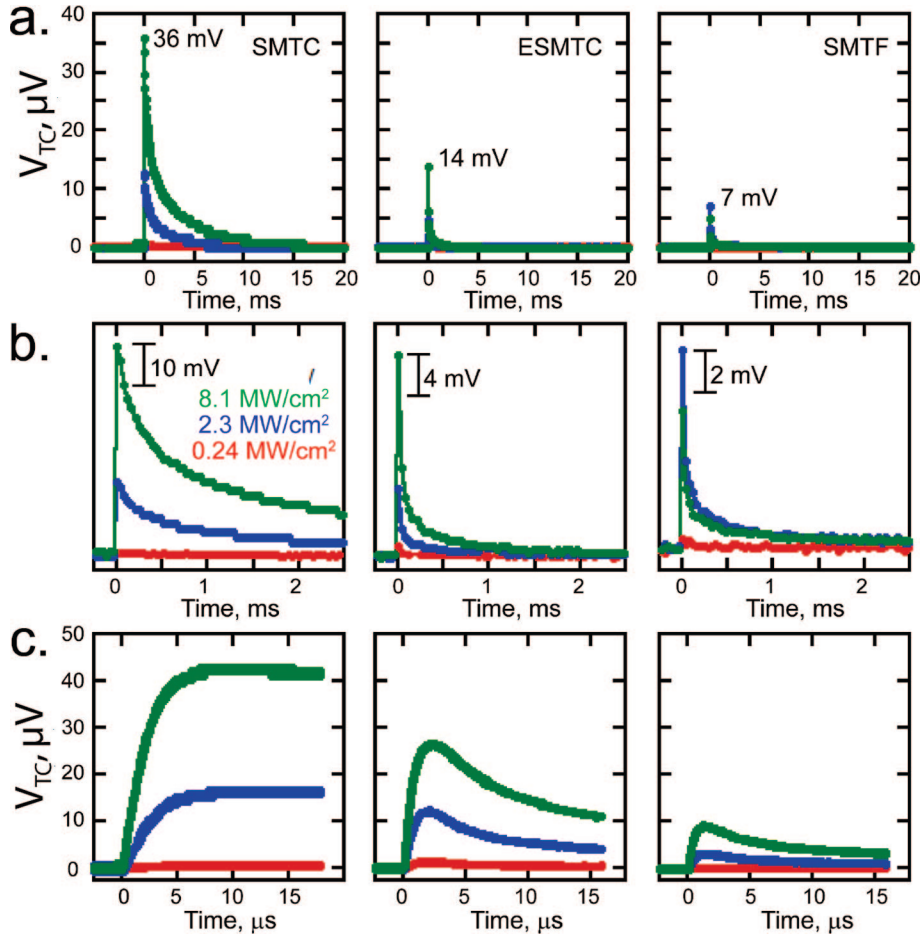

Figure 10. Pulsed laser response time measurements: (a) V_{TC} transients (not normalized) on a 20 ms time scale for a Ag/Ni SMTC (left plot), a Ag/Ni ESMTC (middle plot), and a Ag/Ni SMTF TC (right plot) at peak power densities of 8.1 MW/cm^2 (green), 2.3 MW/cm^2 (blue), and 0.24 MW/cm^2 (red). (b) V_{TC} transients (not normalized) of the same TCs shown in (a), but on a 2.5 ms time scale. (c) V_{TC} transients (not normalized) on a 15 μs time scale for a Ag/Ni SMTC (left plot), a Ag/Ni ESMTC (middle plot), and a Ag/Ni SMTF (right plot).

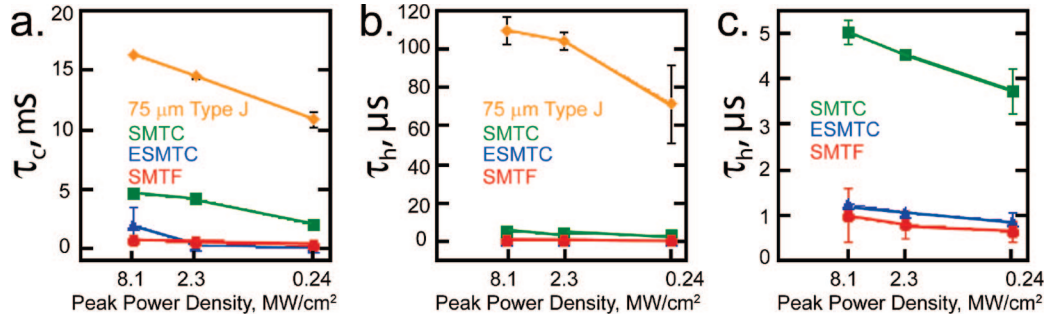

Figure 11. (a) Average decay time versus peak power density for 75 μm type J TCs, Ag/Ni SMTF TCs, Ag/Ni SMTCs, and Ag/Ni ESMTCs. (b) Average rise time versus peak power density for 75 μm type J TCs, Ag/Ni SMTF TCs, Ag/Ni SMTCs, and Ag/Ni ESMTCs. (c) Average rise time versus peak power density for Ag/Ni SMTF TCs, Ag/Ni SMTCs, and Ag/Ni ESMTCs.

time scale (Figure 10c). The smaller output voltages for the SMTF TCs could be due to the highly reflective metal thin film, which would result in a smaller heat input into the TC, as compared to that in SMTCs and ESMTCs. It is interesting to observe the effect the etching has on the shape of the voltage transients. Introducing nanometer-sized contacts between the submicrometer silver particles appears to make the ESMTCs behave more like SMTF TCs. In less than 5 μs the ESMTC has already started to dissipate its heat to the environment, while the SMTC retains a steady-state temperature and only starts to dissipate its heat to the environment after 15 μs (Figure 10c). However, after this initial heat dissipation, the ESMTC dissipates its heat to the surrounding environment at a much slower rate than the SMTF. The similarity in the time scale for the initial heat dissipation can be explained by the thermal decoupling of the junction from the submicrometer silver wires due to etching. This enables the bulk of the initial heating to be dissipated directly from the junction to the cyanoacrylate. After this initial dissipation, the heat is conducted from the junction to the thermoelements and is then radiated to the cyanoacrylate adhesive, similar to the mechanism for SMTCs.

The ability of SMTF TCs to dissipate heat much quicker than those of SMTCs and ESMTCs is a direct result of the surrounding conductive metal thin film.

Interestingly, the rise time is independent of the power density, at least in the range examined in this experiment (Figure 11b,c). There is a decrease in the average rise time with a decrease in power density; however, the values are within the standard deviation. A peak power density of 0.236 MW/cm^2 is at the lower limit of the output of the laser, and therefore the output is not extremely stable, which resulted in an increase in the magnitude of the error. The effect of power density on the decay time is shown in Figure 11a. It is evident that there is a direct correlation between the power density and decay time for all TCs except for the SMTF TCs. The decay time for the SMTF TCs is extremely fast due to the dissipation of heat through the surrounding metal thin film. Therefore, a higher power density would need to be used to reveal an effect on the decay time; however, the stability of the cyanoacrylate at higher power densities would be an issue.

IV. Summary

The main conclusions of this study were the following:

1. Ensembles of Ag/Ni thermocouples consisting of end-butted submicrometer wires can be prepared by coupling electrochemical step edge decoration with a masking strategy in which wire electrodeposition is performed successively, silver first and then nickel (Figure 2b). Precise alignment of the two wire segments at each junction is ensured by the fact that both wire segments nucleate at the same step edge defect. An important aspect of this method is control of spurious deposition of the second metal (in this case, nickel). We found that modification of silver wires with a 1-decanethiol monolayer effectively suppressed the electrodeposition of nickel on the pre-existing silver wires. This thiol monolayer did not, however, interfere with the establishment of an intimate Ag/Ni junction during the electrodeposition of the nickel wire segments.

2. These electrodeposited TC junctions produced linear V_{TC} versus temperature calibration curves characterized by Seebeck coefficients that were identical to the expected values based on the known bulk thermopowers of these two metals (21 μV/°C). Hysteresis in cooling and heating traces was not observed for modest heating and cooling rates in the 0.017 °C/s range. The long-term stability of a small number of devices was also assessed after 1 month of exposure to laboratory air, which resulted in decreases in the Seebeck coefficient of −4% for SMTCs and −10% for ESMTCs.

3. The response times for these TCs—both SMTCs and ESMTCs—estimated using pulsed Nd:YAG lasers, were in the low microsecond range. Somewhat faster response times were seen for ESMTCs in which the silver wires were etched prior to the deposition of nickel nanowire segments. These values compare favorably with those of many TFTCs devices (Figure 1, Table 1) in spite of the fact that the wires, with diameters of 500−800 nm, are still relatively large.

Based upon eq 1, junctions of 10 nm metal wires should yield response times 0.0001 of those seen in this study—easily in the sub-1.0 ns regime. However, these devices may ultimately suffer from the same sensitivity losses already seen for TFTCs in prior studies. Such devices may be accessible using other nanofabrication methods, but the ESED method employed here will not be capable of producing nanowires in this size regime.

A clear disadvantage of our fabrication method is that the number and position of wires on the HOPG surface cannot be controlled for a particular graphite surface. Instead, these attributes are dictated by the number and orientation of step edge defects on that surface. We are also unable to completely suppress the nucleation of metal particles on terraces, away from step edges as seen for example in Figure 3b. In some of the thousands of thermocouples produced in a typical experiment, it is highly likely that these "parasitic" metal particles contribute to the thermal mass of TC junctions when these particles grow into electrical contact with TC junctions. These deficiencies provide motivation to refine the nanofabrication method reported here.

Acknowledgment. This work was funded by the National Science Foundation (Grant CHE-0641169) and the Petroleum Research Fund of the American Chemical Society (Grant 46815-AC10). A.G.G. gratefully acknowledges economical support from the Department of Universities, Research and Information Society (DURSI) of the Catalonia Government through Grant 2005-BE-00730. Graphite for this work was supplied by a grant from the EU Commission FP6 NMP-3 project 505457-1 ULTRA-1D.

CM800582P